scientific reports

OPEN

Manipulation of Majorana bound states in proximity to a quantum ring with Rashba coupling

Fabián Gonzalo Medina[1,4✉], Dunkan Martínez[2,4], Álvaro Díaz-Fernández[3], Francisco Domínguez-Adame[2], Luis Rosales[1] & Pedro A. Orellana[1]

The quest for Majorana zero modes in the laboratory is an active field of research in condensed matter physics. In this regard, there have been many theoretical proposals; however, their experimental detection remains elusive. In this article, we present a realistic setting by considering a quantum ring with Rashba spin-orbit coupling and threaded by a magnetic flux, in contact with a topological superconducting nanowire. We focus on spin-polarized persistent currents to assess the existence of Majorana zero modes. We find that the Rashba spin-orbit coupling allows for tuning the position of the zero energy crossings in the flux parameter space and has sizable effects on spin-polarized persistent currents. We believe that our results will contribute towards probing the existence of Majorana zero modes.

Majorana fermions remain a theoretical construct in the realm of particle physics. These particles, whose main feature is to be their own antiparticles, have been sought after in neutrinos, although without success thus far[1,2]. In condensed matter physics, Majorana quasiparticles emerge in *p*-wave topological superconductors[3,4]. Of particular relevance are the so-called Majorana zero modes (MZM)[2], which are zero-energy Majorana quasi-particles protected by particle-hole symmetry. These quasiparticles, in contrast to their particle counterparts, exhibit yet another crucial feature. Such property is their being non-Abelian under braiding, which renders these quasiparticles as ideal candidates to perform topological quantum computing[5,6]. The reason for this stems in the large degeneracy found in the ground state of a system comprising a large number of Majorana quasiparticles. This degeneracy occurs due to these zero modes being pinned to zero energy[4].

The archetypal model for studying Majorana modes in superconductors is that of Kitaev[7–9], where a one-dimensional spinless *p*-wave superconductor is considered. Under suitable tuning of parameters, the model predicts that an ordinary superconductor undergoes a topological quantum phase transition into a topological superconductor. When considering open boundary conditions, the model predicts an odd number of MZMs at both ends of the chain with exponential decay into the bulk. Kitaev's model, although simple, poses significant challenges for its experimental realization. However, a great deal of experimental advances have taken place during the last few years, and a convenient setting has been put forward[4,10–12]. Such a setting has three key ingredients: a semiconductor nanowire with large spin-orbit coupling, such as InAs and InSb, a uniform magnetic field parallel to the wire to induce Zeeman splitting, and an *s*-wave superconductor such as Al. When placed in contact with the semiconductor and applying the magnetic field, the superconductor becomes topological when a given magnetic field is reached.

In this paper, we consider a superconducting nanowire in the topological regime placed in contact to a quantum ring. We assume the ring to be a continuation of the nanowire, as was done with a quantum dot in Ref.[13], and therefore it displays strong spin-orbit coupling. The ring is in fact a collection of quantum dots assembled in a ring-like fashion, which can be achieved by means of gate voltages. The main results of this paper relate to the impact of the nanowire on the persistent spin currents of the ring, which are sharply different from those of the ring. As we shall show, when the MZMs interact via the quantum ring, they split from zero energy and oscillate, forming zero energy crossings. These crossings reshape the spin currents that would be present in the absence of Majoranas. Therefore, we believe our proposal could potentially be used as an additional tool to uncover the nature of MZMs.

[1]Departamento de Física, Universidad Técnica Federico Santa María, Casilla 110 V, Valparaíso, Chile. [2]GISC, Departamento de Física de Materiales, Universidad Complutense, 28040 Madrid, Spain. [3]GISC, GSC, Departamento de Estructuras y Física de Edificación, Universidad Politécnica de Madrid, 28031 Madrid, Spain. [4]These authors contributed equally: Fabián Gonzalo Medina and Dunkan Martínez. ✉email: fmmedinacfabian@gmail.com
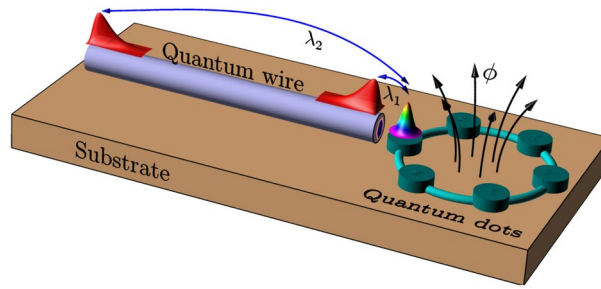
Figure 1. (**a**) Schematic representation of the system under study. A nanowire driven into a superconducting regime supports a MZM at each edge and influences the persistent currents of a quantum ring, threaded by a magnetic flux. (**b**) The quantum ring consists of an array of quantum dots uniformly distributed on a circumference. The MZMs are assumed to be coupled to the same quantum dot of the ring, with coupling constants λ_1 and λ_2.

System and model Hamiltonian

The system under consideration consists of a topological superconducting nanowire hosting MZMs at its edges, as depicted in Fig. 1a. The nanowire is placed in close proximity to a quantum ring, which is threaded by a magnetic flux. We introduce a minimal model that captures the influence of the MZMs on the persistent currents of the ring. The quantum ring consists of an array of quantum dots uniformly distributed on a circumference, as shown in Fig. 1b. Due to the similarities of our system with the one considered in Refs.[12,13], we believe that our model might be amenable to be performed experimentally.

The model Hamiltonian is then given by

$$H = H_r + H_M + H_c ,\tag{1}$$

where H_r is the Hamiltonian of the ring, H_M describes the interaction between the two MZMs at the edges of a nanowire in the topological superconducting regime, and H_c contains the coupling between the MZMs and the quantum ring. Considering spin-orbit coupling and the fact that the quantum ring is threaded by a flux Φ, H_r can be written as[14–16]

$$H_r = -\sum_n \left[\boldsymbol{c}_n^\dagger \big(\boldsymbol{t} + \boldsymbol{t}_{\mathrm{so}}(n)\big) e^{i\theta} \boldsymbol{c}_{n+1} + \text{h.c.} \right] ,\tag{2}$$

where $\boldsymbol{c}_n^\dagger = \left(c_{n,\uparrow}^\dagger, c_{n,\downarrow}^\dagger \right)$ are the creation operators of the quantum ring and n runs from 1 to N, with N the number of sites of the ring, that is, the number of quantum dots that compose it. We shall measure energies in units of $2t$ with t the hopping energy, which implies that $\boldsymbol{t} = \sigma_0/2$, with σ_0 the 2×2 identity matrix. The flux is accounted for in the phase factor $\theta = 2\pi \Phi/N$, where $\Phi = \phi/\phi_0$ is the flux ϕ measured in units of the flux quantum $\phi_0 = h/e$. The spin-orbit coupling is given by

$$\boldsymbol{t}_{\mathrm{so}}(n) = i \tilde{\alpha} \big(\sigma_x \cos \varphi_n + \sigma_y \sin \varphi_n \big) ,\tag{3}$$

where we only consider Rashba spin-orbit interaction, disregarding a possible Dresselhaus interaction[15]. Here, σ_x and σ_y are the Pauli matrices, $\tilde{\alpha} = \alpha N/2\pi R$ being R the radius of the ring, α the strength of the Rashba interaction and

$$\varphi_n = \frac{2\pi}{N} \left(n - \frac{1}{2} \right) .\tag{4}$$

Regarding the mutual coupling between MZMs and the coupling between MZMs and the ring, we will consider a low energy theory as in Ref.[17]. Thus, the interaction term between the two MZMs is given by the minimal Kitaev Hamiltonian for the topological phase[7]

$$H_M = i \xi_M \gamma_1 \gamma_2 ,\tag{5}$$

where γ_1 and γ_2 are Majorana operators which satisfy $\gamma_i = \gamma_i^\dagger$ and $\{\gamma_i, \gamma_j\} = \delta_{ij}$. Here $\xi_M \propto e^{-L/\ell_0}$ where L is the length of the nanowire and ℓ_0 is the superconducting coherence length[7]. The Majorana operators can also be written in terms of ordinary fermion operators, f and $f^\dagger$, as

$$\gamma_1 = \frac{1}{\sqrt{2}}(f + f^\dagger) , \quad \gamma_2 = \frac{i}{\sqrt{2}}(f - f^\dagger) .\tag{6}$$

In terms of these operators, Eq. (5) takes the form

$$H_M = \xi_M \left(f^\dagger f - \frac{1}{2} \right) . \tag{7}$$

Finally, the coupling between the MZMs and the quantum ring is given by[17–19]

$$H_c = \lambda_1 \left(c_{1,\uparrow}^\dagger - c_{1,\uparrow} \right) \gamma_1 + i \lambda_2 \left(c_{1,\uparrow}^\dagger + c_{1,\uparrow} \right) \gamma_2 , \tag{8}$$

where λ_1 and λ_2 are real parameters [see also Fig. 1]. We have chosen to couple the MZMs to a single spin. This can be achieved by fixing the spin canting angles of the MZMs accordingly, which can be done by means of sufficiently large magnetic fields[17]. Finally, we will not consider electron-electron interactions in the ring, which could be included within a mean field approximation[16,17].

It is now convenient to turn to a representation where H_r is diagonal. For that matter, we can use the following unitary transformation[15]

$$\mathscr{U}_n = \frac{1}{\sqrt{2}} \begin{pmatrix} 1 & -1 \\ e^{i\varphi_n} & e^{i\varphi_n} \end{pmatrix} , \tag{9}$$

so that $\mathbf{c}_n = \mathscr{U}_n \tilde{\mathbf{c}}_n$. This transformation turns H_r into

$$H_r = -\sum_n \left(\tilde{\mathbf{c}}_n^\dagger \mathscr{M} e^{i\theta} \tilde{\mathbf{c}}_{n+1} + \text{h.c.} \right) . \tag{10}$$

where

$$\mathscr{M} = e^{i\pi/N} \begin{pmatrix} \left(\frac{1}{2} + i\tilde{\alpha} \right) \cos \left(\frac{\pi}{N} \right) & \left(\frac{i}{2} - \tilde{\alpha} \right) \sin \left(\frac{\pi}{N} \right) \\ \left(\frac{i}{2} + \tilde{\alpha} \right) \sin \left(\frac{\pi}{N} \right) & \left(\frac{1}{2} - i\tilde{\alpha} \right) \cos \left(\frac{\pi}{N} \right) \end{pmatrix} . \tag{11}$$

Notice that the unitary transformation has eliminated the site dependence in the hopping matrix in Eq. (10). Thus, by Fourier transforming H_r we can block-diagonalize it

$$H_r = \sum_k \tilde{\mathbf{c}}_k^\dagger \tilde{\mathbf{h}}_k \tilde{\mathbf{c}}_k , \tag{12}$$

with

$$\tilde{\mathbf{h}}_k = -\cos \left(\frac{\pi}{N} \right) \cos \left(k + \theta + \frac{\pi}{N} \right) \sigma_0 + \sin \left(k + \theta + \frac{\pi}{N} \right) \left[\sin \left(\frac{\pi}{N} \right) \sigma_x - 2\tilde{\alpha} \sin \left(\frac{\pi}{N} \right) \sigma_y + 2\tilde{\alpha} \cos \left(\frac{\pi}{N} \right) \sigma_z \right] . \tag{13}$$

In the basis that diagonalizes $\tilde{\mathbf{h}}_k$ we can write H_r as

$$H_r = \sum_{n,\mu=\pm} \varepsilon_{n\mu} d_{n\mu}^\dagger d_{n\mu} , \tag{14}$$

where the eigenvalues are

$$\varepsilon_{n,\pm} = -\cos \left(\frac{\pi}{N} \right) \cos \left[\frac{2\pi}{N} \left(n + \frac{1}{2} + \Phi \right) \right] \pm \sin \left[\frac{2\pi}{N} \left(n + \frac{1}{2} + \Phi \right) \right] \sqrt{\sin^2 \left(\frac{\pi}{N} \right) + 4\tilde{\alpha}^2} . \tag{15}$$

In this basis, H_c is written as follows

$$H_c = \sum_{n,\mu=\pm} \left[\beta_{n,\mu} d_{n,\mu}^\dagger \left(\lambda_- f^\dagger + \lambda_+ f \right) - \beta_{n,\mu}^* d_{n,\mu} \left(\lambda_- f + \lambda_+ f^\dagger \right) \right] , \tag{16}$$

where $\lambda_\pm = (\lambda_1 \pm \lambda_2)/2$, $\beta_{n,-} = e^{-i 2\pi n/N} (\psi_-^u - \psi_+^u)$, $\beta_{n,+} = e^{-i 2\pi n/N} (\psi_-^d - \psi_+^d)$ with

$$\psi_\pm^u = u_\pm / \sqrt{1 + |u_\pm|^2} ,$$
$$\psi_\pm^d = 1 / \sqrt{1 + |u_\pm|^2} ,$$
$$u_\pm = \frac{2\tilde{\alpha} \cos \left(\frac{\pi}{N} \right) \pm \sqrt{\sin^2 \left(\frac{\pi}{N} \right) + 4\tilde{\alpha}^2}}{(1 - 2i\tilde{\alpha}) \sin \left(\frac{\pi}{N} \right)} . \tag{17}$$

We can now find the spectrum of H by using the Bogoliubov-de Gennes (BdG) Hamiltonian. Indeed, if we introduce

$$\mathbf{\Psi} = \left(\{d_{n,\mu}\}, f, \{d_{n,\mu}^\dagger\}, f^\dagger \right)^T , \tag{18}$$

with $\{d_{n,\mu}\} = d_{1,-}, d_{1,+}, \ldots, d_{N,-}, d_{N,+}$ and likewise for $\{d_{n,\mu}^\dagger\}$, we can write H as
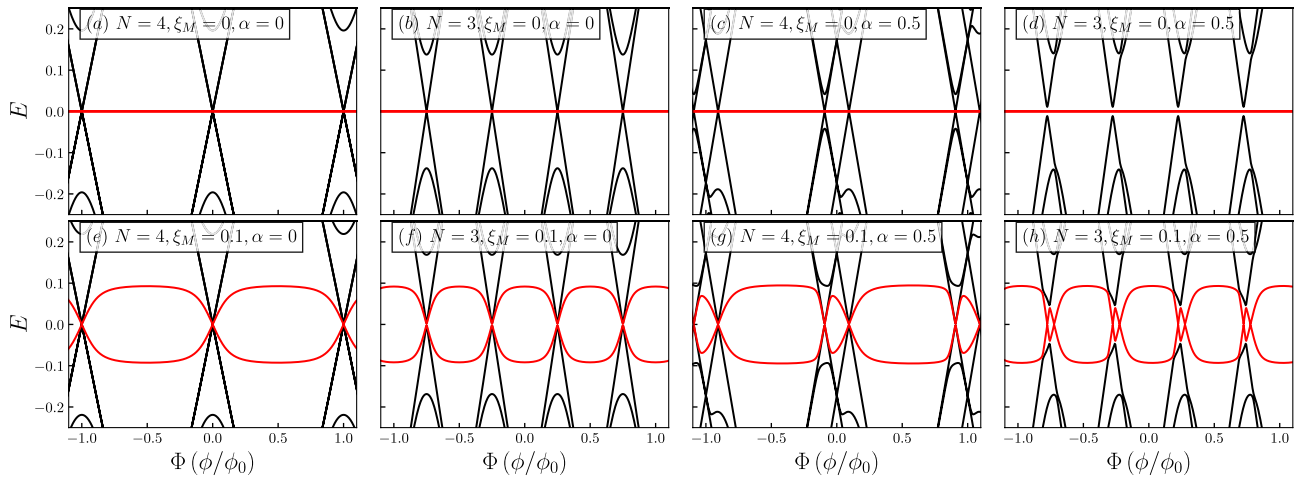
Figure 2. Quasiparticle spectra for $\lambda_1 = 0.1$ and $\lambda_2 = 0$. The number of sites, N, the coupling between MZMs, ξ_M, and the Rashba spin-orbit coupling, α, are indicated in the figure. Black curves represent the states in the quantum ring and the red curves correspond to the Majorana modes.

$$H = \frac{1}{2}\boldsymbol{\Psi}^\dagger \mathscr{H}_{\text{BdG}}\boldsymbol{\Psi}, \tag{19}$$

where

$$\mathscr{H}_{\text{BdG}} = \begin{pmatrix} \mathscr{H} & \Lambda \\ -\Lambda^* & -\mathscr{H}^* \end{pmatrix}, \tag{20}$$

is the BdG Hamiltonian. Here, $\mathscr{H} = \mathscr{H}_0 + \mathscr{V}$ and Λ are the following $(2N+1) \times (2N+1)$ matrices

$$\mathscr{H}_0 = \text{diag}\big[\varepsilon_{1,-}, \varepsilon_{1,+}, \ldots, \varepsilon_{N,-}, \varepsilon_{N,+}, \xi_M\big] \tag{21}$$

$$\mathscr{V} = \lambda_+ \left(\begin{array}{ccccc|c} & & & & & \beta_{1,-} \\ & & & & & \beta_{1,+} \\ & & \mathbf{0}_{2N} & & & \vdots \\ & & & & & \beta_{N,-} \\ & & & & & \beta_{N,+} \\ \hline \beta_{1,-}^* & \beta_{1,+}^* & \cdots & \beta_{N,-}^* & \beta_{N,+}^* & 0 \end{array} \right) \tag{22}$$

$$\Lambda = \lambda_- \left(\begin{array}{ccccc|c} & & & & & \beta_{1,-} \\ & & & & & \beta_{1,+} \\ & & \mathbf{0}_{2N} & & & \vdots \\ & & & & & \beta_{N,-} \\ & & & & & \beta_{N,+} \\ \hline -\beta_{1,-} & -\beta_{1,+} & \cdots & -\beta_{N,-} & -\beta_{N,+} & 0 \end{array} \right) \tag{23}$$

where $\mathbf{0}_{2N}$ is the $2N \times 2N$ zero matrix. The BdG Hamiltonian leads to a particle-hole redundancy and, as a result, the spectrum will be symmetrical around $E = 0$. Diagonalization of $\mathscr{H}_{\text{BdG}}$ provides us with the quasiparticle spectrum, $E(\Phi)$.

Quasiparticle energy spectra

In Figs. 2 and 3, we show the quasiparticle spectrum for rings with $N = 3$ and $N = 4$. The spectra for larger values of N is provided in the Supplemental Material S1, and restrict to $N = 3$ and 4 in the remaining of the text. This is mainly for practical reasons, since the larger the number of dots, the harder an experimental implementation would prove to be.. In the following, we consider two scenarios, namely $\lambda_1 = 0.1$, $\lambda_2 = 0$ and $\lambda_1 = 0.1$, $\lambda_2 = 0.15$, respectively. As explained in Ref.[13], the quantity $\eta = \sqrt{\lambda_2/\lambda_1}$ provides a measure of locality and, as reported in that reference, a value of $\eta \ll 1$ corresponds to highly nonlocal Majoranas, whereas the Majorana components of an Andreev bound state have $\eta \simeq 1$. Since in our case λ_1 and λ_2 are interchangeable, we can see that the values chosen are in the nonlocal regime, that is, $\eta < 1$. In Figs. 2a,b,e,f, we consider the case of $\alpha = 0$ and coupling to a single Majorana mode, namely to γ_1. In this case, we can observe that the spectrum is symmetric as $E(\Phi) = E(-\Phi)$ and the Majorana modes remain at zero energy [see panels (a) and (b)] as long as there is no
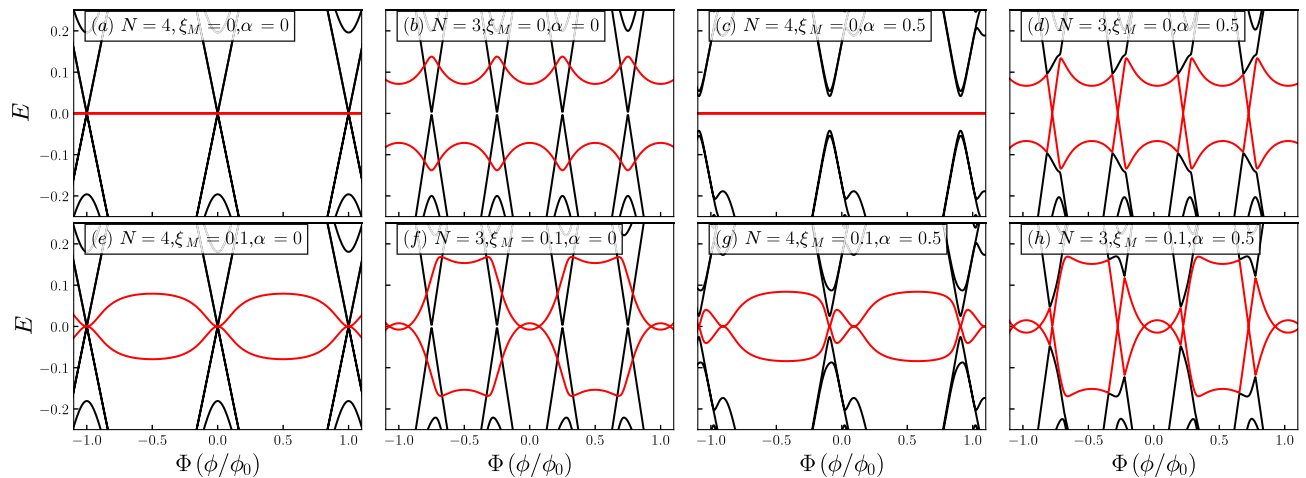
Figure 3. Quasiparticle spectra for $\lambda_1 = 0.1$ and $\lambda_2 = 0.15$. The number of sites, N, the coupling between MZMs, ξ_M, and the Rashba spin-orbit coupling, α, are indicated in the figure. Black curves represent the states in the quantum ring and the red curves correspond to the Majorana modes.

coupling between them, that is, as long as $\xi_M = 0$. However, the coupling to γ_1 breaks the double degeneracy that would otherwise be present in the Dirac cone-like features of the spectra, as can be observed at zero flux. Notice that the degeneracy is lifted only for the spin-up bands, as can be understood from the coupling of the MZMs to the quantum ring in Eq. (8). Nevertheless, this coupling does not lift extra degeneracies, as we shall show when adding Rashba spin-orbit coupling. Once the coupling between MZMs is introduced [see panels (e) and (f)], we see the Majorana oscillations that naturally arise in finite-sized nanowires [2]. There are high symmetry points of the spectrum, namely at the Dirac points, where the hybridization between MZMs effectively vanishes. In panels (c), (d), (g) and (h), while the ring is still coupled to a single MZM, we introduce Rashba spin-orbit coupling. It can be observed that the effect corresponds to a lateral shift of the bands, as expected when Rashba spin-orbit interaction is present. It can be noticed, as we anticipated above, that only certain degeneracies are lifted by the coupling to the Majorana mode. Indeed, for $N = 4$ we can see that the band that shifts to the left-hand side displays both gapless and gaped Dirac-like spectra close to zero energy, while the band that moves rightwards only shows a Dirac cone-like feature. However, for $N = 3$ we can see that the two shifted sides present a gaped Dirac-like spectra; this is because the Rashba spin-orbit coupling makes possible the interaction between MZMs and spin down. This shift is also observed in the oscillatory behavior of the MZMs as they are coupled together. However, these shifts follow the Dirac points corresponding to the spin-up states to which γ_1 is coupled, as we can observe in panels (g) and (h).

In Fig. 3a,b,e,f, we consider the effect of coupling between the two MZMs while keeping the Rashba spin-orbit coupling turned off, $\alpha = 0$. As we can observe, the degeneracy is further lifted by coupling the ring to the two MZMs, as can be observed at zero flux. However, as we expressed above, it is not entirely lifted since there are still gapless Dirac-like features at low energy. It is interesting to notice that there is a clear distinction between even- and odd-numbered rings. Indeed, even when the MZMs are explicitly uncoupled in the Hamiltonian, when $\xi_M = 0$, there is hybridization due to their coupling through the ring. Although we do not show it here, this behavior can be seen to occur in rings with a larger number of sites. This effect may be due to the fact that even-numbered rings with $\alpha = 0$ and at zero flux present particle-hole symmetry $c_{n,\sigma} \to (-1)^n c_{n,-\sigma}^\dagger$ and $c_{n,\sigma}^\dagger \to (-1)^n c_{n,-\sigma}$, whereas odd-numbered rings do not, making these two systems inherently different. Notice that this particle-hole symmetry is a true symmetry, whereas the particle-hole symmetry of the BdG Hamiltonian is a redundancy. Finally, in panels (c), (d), (g) and (h), we show the effect of including Rashba spin-orbit coupling, which breaks the symmetry $E(\Phi) = E(-\Phi)$ by shifting sideways the bands, as occurred in panels (c), (d), (g) and (h) of Fig. 2. However, in contrast to the latter, the coupling to γ_2 leads to a further reduction of the degeneracies in the problem. In fact, for $N = 4$, the spectrum is wholly gaped out, even for $\xi_M = 0$. There is then a clear distinction with the corresponding spectrum without Rashba spin-orbit coupling, which will affect the persistent currents, as we shall show below.

Charge and spin persistent currents

Persistent currents have been studied extensively, both theoretically[16,20–25] and experimentally[26–29]. They constitute a peculiar quantum phenomenon resulting from the time-reversal symmetry breaking that occurs from coupling electrons to a gauge field, as in the Aharonov-Bohm effect.

In this section, we will study the appearance of persistent charge, I_q, and spin currents, I_s, in all the scenarios discussed above. We will calculate I_q as

$$I_q = -i \left\langle \left[N_\uparrow + N_\downarrow, H_r \right] \right\rangle, \tag{24}$$

and I_s as

$$I_s = -\mathrm{i} \left\langle \left[N_\uparrow - N_\downarrow, H_r \right] \right\rangle, \tag{25}$$

where $N_\sigma = \sum_n c_{n,\sigma}^\dagger c_{n,\sigma}$. Notice that the charge persistent current can also be obtained from the eigenenergies E_ν by summing over all states $I_q = \sum_\nu I_{q,\nu}$ where[16]

$$I_{q,\nu} = -\frac{\partial}{\partial \Phi} \left[f(E_\nu) E_\nu \right], \tag{26}$$

and $f(E_\nu)$ the Fermi distribution function. The total persistent current is obtained by summing over all states [16]. After lengthy but straightforward calculations, we find that

$$I_{q(s)} = -\sum_n \left[\chi_n^{q(s)} + \gamma_n^{q(s)} - \chi_n^{q(s)} \langle d_{n,-} d_{n,-}^\dagger \rangle - \gamma_n^{q(s)} \langle d_{n,+} d_{n,+}^\dagger \rangle - 2\mathrm{Re} \left\{ \beta_n^{q(s)} \langle d_{n,+} d_{n,-}^\dagger \rangle \right\} \right]. \tag{27}$$

As we can see, the expressions for the persistent currents are identical, except for the coefficients. For the charge persistent current, we find

$$
\begin{aligned}
\chi_n^q &= A_n^+ \left| \psi_-^u \right|^2 + A_n^- \left| \psi_+^u \right|^2 + 2\mathrm{Re} \left\{ B_n \psi_-^u \left(\psi_+^u \right)^* \right\}, \\
\gamma_n^q &= A_n^+ \left| \psi_-^d \right|^2 + A_n^- \left| \psi_+^d \right|^2 + 2\mathrm{Re} \left\{ B_n \psi_-^d \left(\psi_+^d \right)^* \right\}, \\
\beta_n^q &= A_n^+ \psi_-^u \left(\psi_-^d \right)^* + A_n^- \psi_+^u \left(\psi_+^d \right)^* + B_n \psi_-^u \left(\psi_+^d \right)^* + B_n^* \psi_+^u \left(\psi_-^d \right)^*,
\end{aligned}
\tag{28}
$$

where

$$
\begin{aligned}
A_n^\pm &= \left[\sin \left(\frac{\pi}{N} + \frac{2\pi}{N}\Phi + \frac{2\pi n}{N} \right) \pm 2\tilde{\alpha} \cos \left(\frac{\pi}{N} + \frac{2\pi}{N}\Phi + \frac{2\pi n}{N} \right) \right] \cos \left(\frac{\pi}{N} \right), \\
B_n &= (1 + i2\tilde{\alpha}) \cos \left(\frac{\pi}{N} + \frac{2\pi}{N}\Phi + \frac{2\pi n}{N} \right) \sin \left(\frac{\pi}{N} \right).
\end{aligned}
\tag{29}
$$

The expressions for the spin persistent current coefficients are identical by replacing $\sin \leftrightarrow \cos$ in $A_n^\pm$ and B_n and by taking $\tilde{\alpha} \to -\tilde{\alpha}$ in B_n. Considering the fluctuation-dissipation theorem, we can write

$$I_{q(s)} = -\sum_n \frac{1}{\pi} \int_{-\infty}^\infty d\omega f(\omega) \left[\chi_n^{q(s)} \mathrm{Im}\langle\langle d_{n,-}; d_{n,-}^\dagger \rangle\rangle_\omega + 2\mathrm{Re}\left\{ \beta_n^{q(s)} \mathrm{Im}\langle\langle d_{n,-}; d_{n,+}^\dagger \rangle\rangle_\omega \right\} + \gamma_n^{q(s)} \mathrm{Im}\langle\langle d_{n,+}; d_{n,+}^\dagger \rangle\rangle_\omega \right]. \tag{30}$$

Here $\langle\langle \ldots \rangle\rangle$ stands for the Green's functions of the ring. Notice that we have dropped the first two terms in Eq. (27), $\chi_n^{q(s)}$ and $\gamma_n^{q(s)}$, since they end up cancelling out. The Green's functions can be obtained by applying the equation of motion technique[30], which are found to be

$$
\begin{aligned}
\langle\langle d_{n,-}; d_{n,-}^\dagger \rangle\rangle &= g_{p,-} + \frac{g_{p,-}^2 |\beta_{n,-}|^2}{\tilde{M}_p \tilde{M}_h - \tilde{S}^2} \left[\lambda_-^2 \tilde{M}_p + \lambda_+^2 \tilde{M}_h + 2\lambda_+ \lambda_- \tilde{S} \right] \\
\langle\langle d_{n,+}; d_{n,+}^\dagger \rangle\rangle &= g_{p,+} + \frac{g_{p,+}^2 |\beta_{n,+}|^2}{\tilde{M}_p \tilde{M}_h - \tilde{S}^2} \left[\lambda_-^2 \tilde{M}_p + \lambda_+^2 \tilde{M}_h + 2\lambda_+ \lambda_- \tilde{S} \right], \\
\langle\langle d_{n,-}; d_{n,+}^\dagger \rangle\rangle &= \frac{g_{p,-} \beta_{n-} g_{p,+} \beta_{n+}^*}{\tilde{M}_p \tilde{M}_h - \tilde{S}^2} \left[\lambda_-^2 \tilde{M}_p + \lambda_+^2 \tilde{M}_h + 2\lambda_+ \lambda_- \tilde{S} \right],
\end{aligned}
\tag{31}
$$

where $g_{p,\pm} = (z - \varepsilon_{n,\pm})^{-1}$ are the Green's functions of the quantum ring in the absence of interaction with the MZMz and

$$
\begin{aligned}
\tilde{M}_p &= z - \xi_M - \sum_n \left(\lambda_-^2 S_h + \lambda_+^2 S_p \right), \\
\tilde{M}_h &= z + \xi_M - \sum_n \left(\lambda_+^2 S_h + \lambda_-^2 S_p \right), \\
\tilde{S} &= \lambda_+ \lambda_- \sum_n \left(|\beta_{n,-}|^2 g_{h,-} + |\beta_{n,+}|^2 g_{h,+} + |\beta_{n,-}|^2 g_{p,-} + |\beta_{n,+}|^2 g_{p,+} \right).
\end{aligned}
\tag{32}
$$

Here $g_{h,\pm} = (z + \varepsilon_{n,\pm})^{-1}$ are the Green's functions for holes of the ring uncoupled to the MZMs. In order to assess the effect of having MZMs, we first show in Fig. 4 the charge and spin persistent currents for the system without MZMs. Additionally, we include the quasiparticle spectra where it can be seen that, as expected, the only effect is a lateral shift, as indicated by solid and dashed lines. Here, panels (b) and (c) correspond to the charge persistent currents for the $N = 3$ and $N = 4$ cases respectively and panels (d) and (e) correspond to the spin persistent currents for the $N = 3$ and $N = 4$ cases respectively. The different colours indicate the value of the Rashba spin-orbit interaction. As it can be noticed, the Rashba interaction leads to a secondary peak in the charge persistent current and to nonzero spin persistent currents.
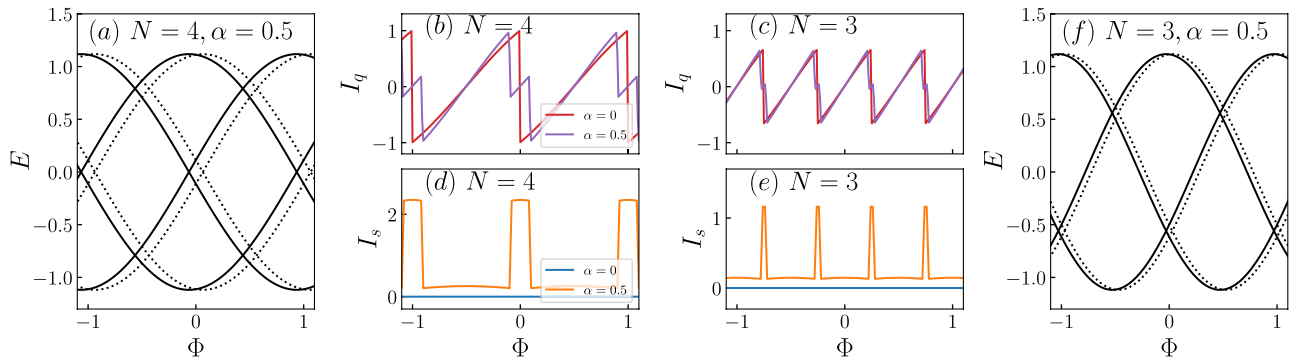
6

Figure 4. Quasiparticle spectra and corresponding charge and spin persistent currents, I_q and I_s respectively, for $\lambda_1 = \lambda_2 = \xi_M = 0$. The number of sites, N, and the Rashba spin-orbit coupling, α, are indicated in the figures.
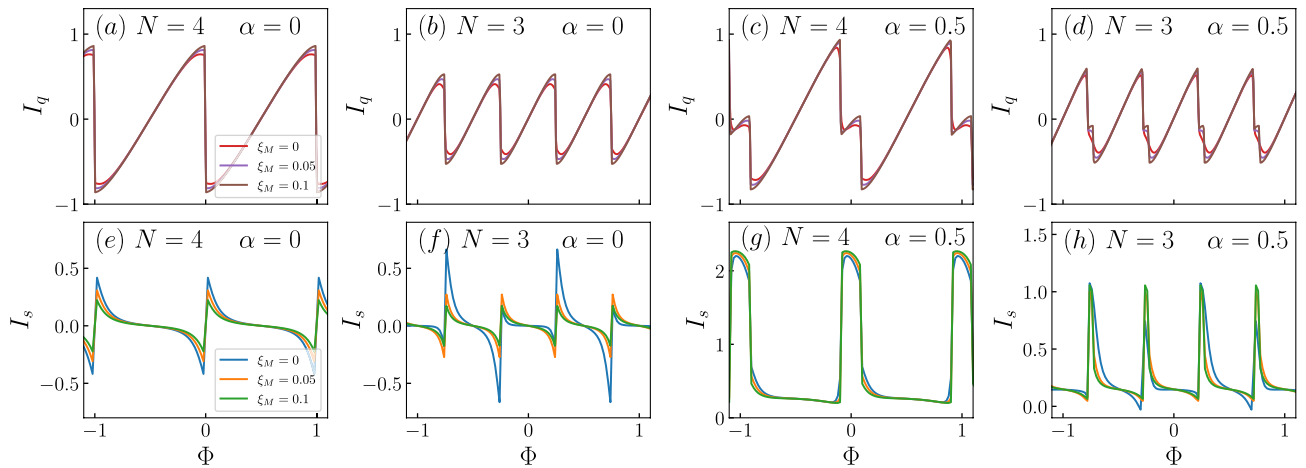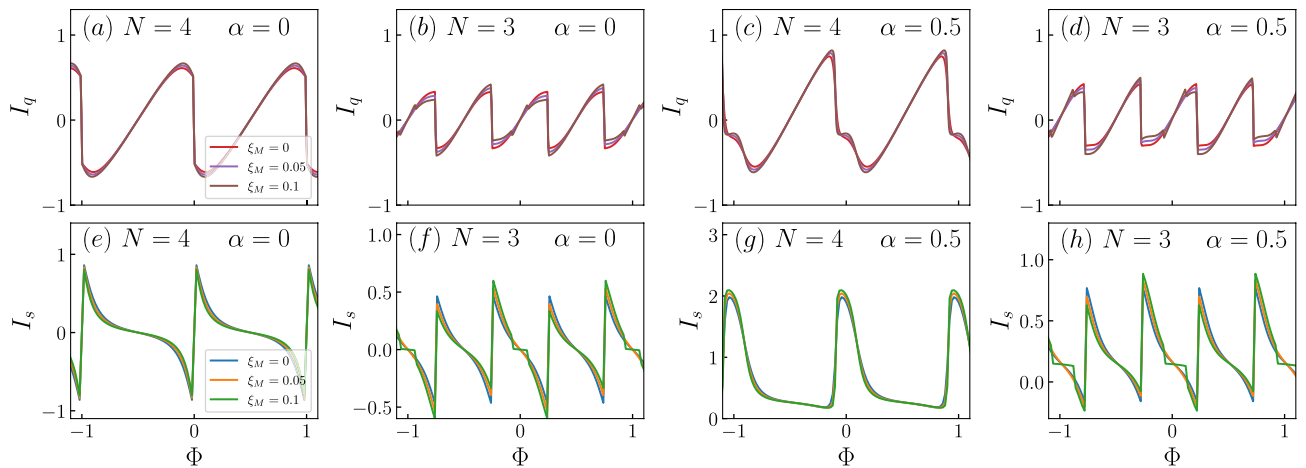

Figure 5. Charge and spin persistent currents, I_q and I_s respectively, for $\lambda_1 = 0.1, \lambda_2 = 0$. The number of sites, N, and the Rashba spin-orbit coupling, α, are indicated in the figures. The coupling between MZMs, ξ_M, is indicated by coloured lines, shown in the leftmost panels.

Figure 6. Charge and spin persistent currents, I_q and I_s respectively, for $\lambda_1 = 0.1, \lambda_2 = 0.15$. The number of sites, N, and the Rashba spin-orbit coupling, α, are indicated in the figures. The coupling between MZMs, ξ_M, is indicated by coloured lines, shown in the leftmost panels.

We now study the persistent currents for the cases discussed in Figs. 2, 3 and obtain Figs. 5, 6. Here we use the same labeling as in the last figure, but the colours indicate three different values of ξ_M, one being $\xi_M = 0$ [panels (a)–(d) in the BdG spectra], another being $\xi_M = 0.1$ [panels (e)–(h) in the BdG spectra] and another one in between, $\xi_M = 0.05$, whose spectrum is not shown.

Figure 5a,b,e,f corresponds to the settings of Fig. 2a,b,e,f. The first thing we observe is that the persistent currents display the periodicity observed in the spectra, as it should. In the case of the charge currents, we can see that upon decreasing the interaction between the two MZMs, the peaks in the current become smoother. On the other hand, the spin currents are nonzero due to the coupling of one of the two MZMs to the up-spin electrons in the ring. However, as the coupling between MZMs increases, reducing their topological robustness, the spin current tends towards zero. This is consistent with the results shown in the Fig. 4 as a greater interaction hybridizes the Majoranas.

Figure 5c,d,g,h refers to the scenario considered in Fig. 2c,d,g,h, which is identical to the previous one except for a nonzero Rashba spin-orbit coupling. As we can see, in this case, the charge current is affected, as signaled by the appearance of additional peaks. Since the position of these peaks depends on the value of α, we can fine-tune the persistent current by manipulating this parameter. However, the sharpest distinction occurs when considering the spin currents. As we can observe, Rashba renders the spin currents asymmetric around zero current and, additionally, it leads to a pulse-like pattern, similar to the one we can see in Fig. 4.

In Fig. 6a,b,e,f we show the persistent currents for the parameters of Fig. 3a,b,e,f. In this case, the Rashba spin-orbit coupling is turned off, but the two MZMs are coupled to the ring. As we can observe, the results for the charge current are not dramatically altered, except for the curves being smoother in the $N = 4$ case and for a secondary peak at $N = 3$ as ξ_M is increased to $\xi_M = 0.1$. These peaks feature in a clearer fashion in the spin currents, where a small plateau for $\xi_M = 0.1$ is observed at certain values of flux. This can be understood from Fig. 3. Take for instance the spectrum around $\Phi = 0$ in panel (f) of that figure. Although it is very subtle, there is a switching of the Majorana states at zero energy and it is in the region between the two crossings where this plateau takes place. Additionally, we can observe that there is no suppression of the spin current upon increasing ξ_M, as there was when $\lambda_2 = 0$. Therefore, we can see that, by coupling the ring to the two MZMs we are able to suppress spin current for a range of fluxes. This could be a smoking gun in the detection of MZMs as this situation is completely different from the result in the absence of MZMs (cf. Fig. 4).

Finally, Fig. 6c,d,g,h corresponds to the case shown in Fig. 3c,d,g,h. In this scenario, the currents are similar to those of panels (a), (b), (e) and (f), but with the additional peak that was observed for $N = 4$ in Fig. 5c, although clearly smoothed out. In fact, the additional peak for the $N = 3$ case is completely suppressed. This has an effect on the spin current, where the $N = 4$ case still shows a pulse-like behaviour, but the $N = 3$ case shows plateaus for a larger range of fluxes than in panels (a), (b), (e) and (f).

Conclusions

MZMs stand out for their remarkable properties in the realm of topological quantum matter, such as their non-Abelian statistics. However, although significant progress has been made in the direction of their experimental detection in recent years, they cannot be confirmed as yet. More importantly, recent discoveries show that it is necessary to carefully examine different effects to determine their existence [31] unambiguously. In this regard, we propose to consider a topological superconducting nanowire in proximity to a quantum ring threaded by a magnetic flux. It is the natural extension of the system presented in Ref. [17] where a nanowire is coupled to a single quantum dot. In addition, we propose the ring to display Rashba spin-orbit coupling. As we have shown in this paper, the BdG spectra are entirely altered by coupling the quantum ring to one or two MZMs and having a nonzero Rashba spin-orbit coupling. The consequences are clearly observed in the persistent currents. Interestingly, spin-orbit coupling leads to an asymmetric spin current with a square pulse-like behavior. Moreover, the coupling to the two MZMs leads to plateaus for odd-numbered rings due to the switching of MZMs at zero energy. We believe that our work could serve as an additional signature towards probing the existence of Majorana zero modes.

References

1. Beenakker, C. Search for Majorana fermions in superconductors. *Annu. Rev. Cond. Matter Phys.* **4**, 113–136 (2013).
2. Aguado, R. Majorana quasiparticles in condensed matter. *La Riv. Nuovo Cimento* **40**, 523–593 (2017).
3. Stanescu, T. D. & Tewari, S. Majorana fermions in semiconductor nanowires: Fundamentals, modeling, and experiment. *J. Phys. Cond. Matter* **25**, 233201 (2013).
4. Lutchyn, R. M. *et al.* Majorana zero modes in superconductor-semiconductor heterostructures. *Nat. Rev. Mater.* **3**, 52 (2018).
5. Sarma, S. . D., Freedman, M. & Nayak, C. Majorana zero modes and topological quantum computation. *NPJ Quant. Inf.* **1**, 15001 (2015).
6. Sato, M. & Fujimoto, S. Majorana fermions and topology in superconductors. *J. Phys. Soc. Jpn.* **85**, 072001 (2016).
7. Kitaev, A. Y. Unpaired Majorana fermions in quantum wires. *Phys. Uspekhi* **44**, 131 (2001).
8. Alicea, J. New directions in the pursuit of Majorana fermions in solid state systems. *Rep. Prog. Phys.* **75**, 076501 (2012).
9. Elliott, S. R. & Franz, M. Colloquium: Majorana fermions in nuclear, particle, and solid-state physics. *Rev. Mod. Phys.* **87**, 137 (2015).
10. Lutchyn, R. M., Sau, J. D. & Das Sarma, S. Majorana fermions and a topological phase transition in semiconductor-superconductor heterostructures. *Phys. Rev. Lett.* **105**, 077001 (2010).
11. Oreg, Y., Refael, G. & von Oppen, F. Helical liquids and Majorana bound states in quantum wires. *Phys. Rev. Lett.* **105**, 177002 (2010).
12. Deng, M. T. *et al.* Majorana bound state in a coupled quantum-dot hybrid-nanowire system. *Science* **354**, 1557 (2016).

13. Deng, M.-T. *et al.* Nonlocality of Majorana modes in hybrid nanowires. *Phys. Rev. B* **98**, 085125 (2018).
14. Liu, X., Borunda, M. F., Liu, X.-J. & Sinova, J. Control of josephson current by Aharonov-Casher phase in a Rashba ring. *Phys. Rev. B* **80**, 174524 (2009).
15. Maiti, S. .K. ., Dey, M., Sil, S., Chakrabarti, A. & Karmakar, S. N. Magneto-transport in a mesoscopic ring with Rashba and Dresselhaus spin-orbit interactions. *EPL Europhys. Lett.* **95**, 57008 (2011).
16. Monisha, P. J., Sankar, I. V., Sil, S. & Chatterjee, A. Persistent current in a correlated quantum ring with electron-phonon interaction in the presence of Rashba interaction and Aharonov–Bohm flux. *Sci. Rep.* **6**, 20056 (2016).
17. Prada, E., Aguado, R. & San-Jose, P. Measuring Majorana nonlocality and spin structure with a quantum dot. *Phys. Rev. B* **96**, 085418 (2017).
18. Zeng, Q.-B., Chen, S., You, L. & Lü, R. Transport through a quantum dot coupled to two Majorana bound states. *Front. Phys.* **12**, 127302 (2017).
19. Ramos-Andrade, J. P., Orellana, P. A. & Ulloa, S. E. Detecting coupling of Majorana bound states with an Aharonov–Bohm interferometer. *J. Phys. Cond. Matter* **30**, 045301 (2018).
20. Byers, N. & Yang, C. N. Theoretical considerations concerning quantized magnetic flux in superconducting cylinders. *Phys. Rev. Lett.* **7**, 46 (1961).
21. Büttiker, M., Imry, Y. & Landauer, R. Josephson behavior in small normal one-dimensional rings. *Phys. Lett. A* **96**, 365 (1983).
22. Ambegaokar, V. & Eckern, U. Coherence and persistent currents in mesoscopic rings. *Phys. Rev. Lett.* **65**, 381 (1990).
23. Riedel, E. K. & von Oppen, F. Mesoscopic persistent current in small rings. *Phys. Rev. B* **47**, 15449 (1993).
24. Orellana, P. A. & Pacheco, M. Persistent current magnification in a double quantum-ring system. *Phys. Rev. B* **71**, 235330 (2005).
25. Maiti, S. K. & Chakrabarti, A. Magnetic response of interacting electrons in a fractal network: A mean-field approach. *Phys. Rev. B* **82**, 184201 (2010).
26. Mailly, D., Chapelier, C. & Benoit, A. Experimental observation of persistent currents in gaas-algaas single loop. *Phys. Rev. Lett.* **70**, 2020 (1993).
27. Jariwala, E. M. Q., Mohanty, P., Ketchen, M. B. & Webb, R. A. Diamagnetic persistent current in diffusive normal-metal rings. *Phys. Rev. Lett.* **86**, 1594 (2001).
28. Bluhm, H., Koshnick, N. C., Bert, J. A., Huber, M. E. & Moler, K. A. Persistent currents in normal metal rings. *Phys. Rev. Lett.* **102**, 136802 (2009).
29. Bleszynski-Jayich, A. C. *et al.* Persistent currents in normal metal rings. *Science* **326**, 272 (2009).
30. Jishi, R. .A. . *Feynman Diagram Techniques in Condensed Matter Physics* (Cambridge University Press, 2013).
31. Frolov, S. Quantum computing's reproducibility crisis: Majorana fermions. *Nature* **592**, 350 (2021).

Acknowledgements

Author contributions

P.A.O., F.D.A. and L.R. conceived the research. F.G.M. and D.M. performed the calculations. A.D.F. carried out calculations and wrote the manuscript. All authors discussed the results and reviewed the manuscript.

Competing interests

The authors declare no competing interests.

Additional information

Supplementary Information The online version contains supplementary material available at https://doi.org/10.1038/s41598-022-05043-y.

Correspondence and requests for materials should be addressed to F.G.M.

Reprints and permissions information is available at www.nature.com/reprints.

Publisher's note Springer Nature remains neutral with regard to jurisdictional claims in published maps and institutional affiliations.